



Ab initio molecular dynamics study of the interlayer and micropore structure of aqueous montmorillonite clays

James L. Suter^a, Lara Kabalan^{a,b}, Mahmoud Khader^c, Peter V. Coveney^{a,*}

^a Centre for Computational Science, University College London, 20 Gordon Street, London WC1H 0AJ, United Kingdom

^b Qatar Environment and Energy Research Institute, Qatar Foundation, PO Box 5825, Doha, Qatar

^c Gas Processing Center, Qatar University, P.O. Box 2713, Doha, Qatar

Received 20 March 2015; accepted in revised form 9 July 2015; available online 15 July 2015

Abstract

Ab initio molecular dynamics simulations have been performed to gain an understanding of the interfacial microscopic structure and reactivity of fully hydrated clay edges. The models studied include both micropore and interlayer water. We identify acidic sites through dissociation mechanisms; the resulting ions can be stabilized by both micropore and interlayer water. We find clay edges possess a complex amphoteric behavior, which depends on the face under consideration and the location of isomorphous substitution. For the neutral (110) surface, we do not observe any dissociation on the timescale accessible. The edge terminating hydroxyl groups participate in a hydrogen bonded network of water molecules that spans the interlayer between periodic images of the clay framework. With isomorphous substitutions in the tetrahedral layer of the (110) clay edge, we find the adjacent exposed apical oxygen behaves as a Brønsted base and abstracts a proton from a nearby water molecule, which in turn removes a proton from an AlOH_2 group. With isomorphous substitutions in the octahedral layer of the (110) clay edge the adjacent exposed apical oxygen atom does not abstract a proton from the water molecules, but increases the number of hydrogen bonded water molecules (from one to two). Acid treated clays are likely to have both sites protonated. The (010) surface does not have the same interfacial hydrogen bonding structure; it is much less stable and we observe dissociation of half the terminal SiOH groups ($\equiv\text{Si}-\text{O}-\text{H} \rightarrow \equiv\text{Si}-\text{O}^- + \text{H}^+$) in our models. The resulting anions are stabilized by solvation from both micropore and interlayer water molecules. This suggests that, when fully hydrated, the (010) surface can act as a Brønsted acid, even at neutral pH.

© 2015 The Authors. Published by Elsevier Ltd. This is an open access article under the CC BY license (<http://creativecommons.org/licenses/by/4.0/>).

1. INTRODUCTION

Smectite clays, such as montmorillonite (MMT), consist of layers of magnesium aluminum silicate separated by galleries of nanoscale thickness (Brindley and Brown, 1980; Murray, 2000; Giese and Van Oss, 2002). The layers are stacked into platelets composed of tens to hundreds of individual layers. The layers possess dimensions of 1 nm thickness and are 100–500 nm in diameter, resulting in platelets

of very high aspect ratio. Isomorphous substitutions in the crystal structure of the clay, such as substitution of Al^{3+} in octahedral sites by Mg^{2+} and Si^{4+} by Al^{3+} in tetrahedral sites produce a net negative surface charge (Sposito et al., 1999). This is counter balanced by exchangeable cations in the interlayer galleries, such as Na^+ and Ca^{2+} (Brindley and Brown, 1980; Newman, 1987).

In humid environments the ions found in the interlayer have a strong tendency to hydrate. Water molecules penetrate between the stacked layers, forcing the layers apart and increasing the clay layer spacing. This interesting characteristic of smectite clays has been utilized in areas such as energy applications (for example, the containment of

* Corresponding author.

E-mail address: p.v.coveney@ucl.ac.uk (P.V. Coveney).

waste), biomedical applications (for the intercalation of bio-molecules) and in materials (the intercalation of polymers to create nano-composites) (Greenwell et al., 2006; Chen et al., 2008). In the oil industry, clay (also known as shale) swelling can cause wellbore instability problems leading to adverse impacts on drilling operations when using water-based drilling fluids (Anderson et al., 2010; Suter et al., 2011). As a result of these diverse application areas, the swelling behavior of clays, and how it can be beneficially modified, represents an active area of research (Chen et al., 2008).

The thermodynamic swelling of clays is related to the tendency of the charge balancing counterions to hydrate, the hydrophilic interaction between the clay surface and water, and the strength of the interaction between the clay surface and the counterion (Boulet et al., 2006). A large body of research has shed light on the properties of the water/clay surface interfaces confined between the basal planes of clay layers (for example, Refs. Karaborni et al. (1996), Delville (1991), Boek et al. (1995), Boek et al. (1995), Bridgeman and Skipper (1997), Chang et al. (1997), Chang et al. (1998), Chang et al. (1995), Marry and Turq (2003), Marry et al. (2008), Rotenberg et al. (2010) and Morrow et al. (2013)). There are also several comprehensive reviews Sposito et al. (1999), Anderson et al. (2010), Cygan et al. (2009) and Bergaya and Lagaly (2013)). However, another important consideration is the edges of the clay layers. These edges exist where, as a result of the finite size of the layers, the crystal structure of the clay ends and the dangling bonds are terminated by hydroxyl sites. Due to the high aspect ratio of clay layers, the edges only comprise a small percentage of the surface of a clay platelet (estimated by Tournassat et al. (2003) to be approximately 1%). For clay swelling to occur, however, water molecules must pass from external regions (such as external surfaces and micropores) into the interlayer gallery, passing between these clay edges. In contrast to the chemically inert basal plane, the edges of clay particles are extremely reactive (Bickmore et al., 2003; Churakov, 2006, 2007; Stackhouse et al., 2001) containing both Brønsted acid and base groups. The reactive nature of clay layer edges has been implicated in catalysis reactions, such as polymerization (Stackhouse et al., 2001; Briones-Jurado and Agacino-Valdés, 2009); the under-coordinated aluminum atoms are expected to act as Lewis acids, activating monomers for reaction. The terminal hydroxyl groups are also relatively mobile, unlike those constrained within the clay framework (Liu et al., 2012). To gain insight into the processes involved in clay swelling, and more generally of water transport between the micropore and the interlayer region, we must understand how the properties of the edges influence the structure and dynamics of water both in the interlayer, micropore and the interface region close to the edges. Similarly, to gain insight into the catalytic properties of clay edges, we need to understand the reactivity of the exposed atoms, especially in the hydrated environment commonly encountered in catalytic reactions.

The reactivity and polarizability of clay edges are best handled through electronic structure calculations. Density functional theory (DFT) provides a first principles

description of the interlayer structure of ions and water (Boek and Sprick, 2003; Suter et al., 2008, 2012) and the structure of clay edges (Bickmore et al., 2003; Churakov, 2006, 2007; Liu et al., 2012; Tazi et al., 2012). DFT can be combined with quantum mechanical molecular dynamics (*ab initio* MD), where the ions are propagated using the potentials calculated from the electronic structure. Such an approach comes at considerable computational cost: system sizes are restricted to less than 1000 atoms and time scales to 10–20 ps. This timescale is usually regarded as sufficient to observe the formation of hydrogen bonds, water reorganization, and proton exchange between acidic edge sites and adsorbed water molecules. *Ab initio* MD is therefore an ideal method for determining the surface geometries, water structure and reactivities of the edge facets of clays. The restriction of length and timescales accessible means that our simulations are only observational: to determine quantitative features, such as dissociation free energies, requires enhanced sampling techniques, free-energy or replica methods, all of which significantly increase the computational costs and are, as such, only possible for much reduced system sizes, where finite size effects can become a concern. The purpose of this current paper is to use unbiased *ab initio* MD to study the clay edge interfacial phenomena on the timescale of *ab initio* MD and infer the qualitative behavior from our observations.

This paper is organized as follows. In Section 2 we introduce the models we use to describe the interlayer/micropore clay interface, each containing different lateral facets of the clay crystal and isomorphic substitutions in the clay framework. We also describe our *ab initio* MD simulation set-up (methods and analysis). In Section 3 we discuss the results of the *ab initio* MD simulations, including the water structure, leading to observation of the Lewis and Brønsted acidities of the clay edges. Finally, in Section 4, we present the conclusions from this study.

2. SIMULATION METHODS

All *ab initio* MD simulations were performed using periodic models containing approximately 500–600 atoms, using the CPMD code (Hutter et al., 2011). To create the edge structures, we follow the procedure used by Churakov (2006). The different faces are formed by cutting the crystal parallel to the selected direction while keeping the crystal stoichiometry unchanged. This was achieved using the Material Studio program (Accelrys Software Inc, 2007). All broken bonds were either terminated using hydrogen atoms or hydroxyl groups. We investigated the (110) surface (and the identical (-110) surface) and the (010) surface. Each simulation supercell therefore contains two edge surfaces (see Fig. 1). The calculations were performed for a $2 \times 1 \times 1$ supercell containing eight formula units of pyrophyllite, corresponding to the formula $\text{Al}_{16}\text{Si}_{32}\text{O}_{80}(\text{OH})_{16}$. A vacuum space of 8 Å was added to the lattice parameter perpendicular to the cleaved surface to reduce the interaction with other periodic units. Similarly, the L_z lattice parameter was increased to 13.5 Å. Our preliminary simulations showed that this spacing was sufficient to create a bilayer of water in the interlayer

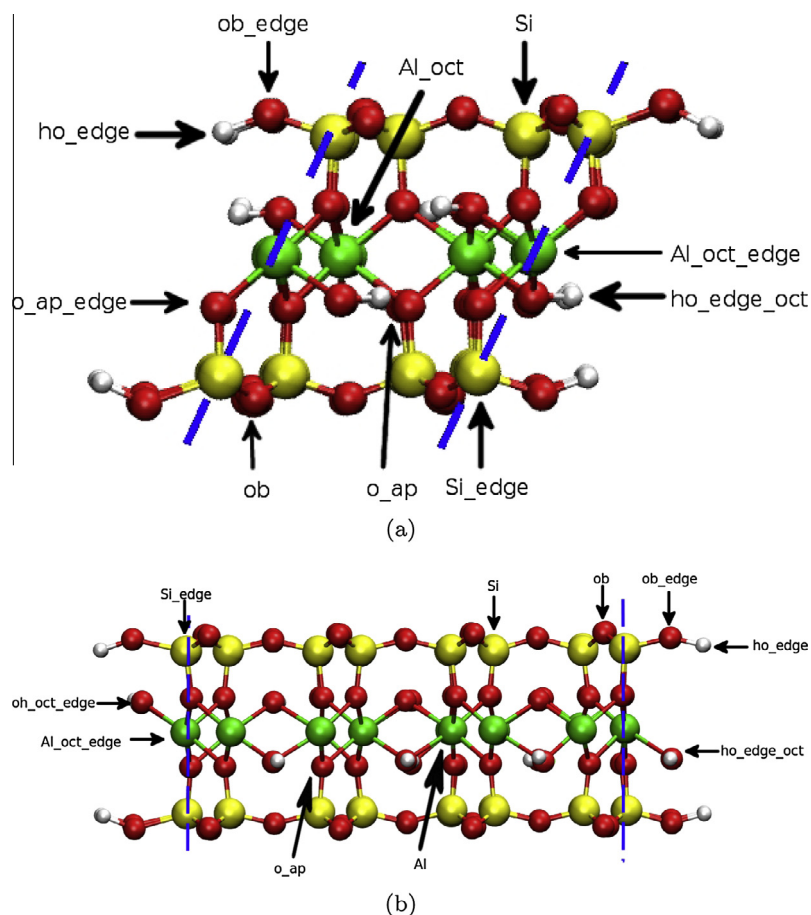


Fig. 1. The starting structure for the neutral clay (a) (110) face viewed in the xz plane and (b) (010) face viewed in the yz plane. The atom colors are as follows: silicon = yellow, oxygen = red, hydrogen = white, aluminium = green. The different atom types found in the structure are identified here. On the (110) face: *ob*_edge are terminal basal oxygen atoms, *ho*_edge are hydrogen atoms on the terminating hydroxyl group, *o*_ap_edge are the exposed apical oxygen atoms, *Al*_oct_edge are octahedral layer aluminium atoms, *ho*_edge_oct are the exposed octahedral layer hydroxyl groups and *Si*_edge are the silicon atoms on the (110) face. On the basal surface: *ob* are the basal oxygen atoms, *Si* are the basal silicon atoms. In the clay framework, *Al*_oct are the octahedral atoms and *o*_ap the apical oxygen atoms. The nomenclature is the same for the (010) face. The density profiles are calculated as distances normal to the nearest (110) face or (010) face, defined by the blue dashed lines, which pass through the corresponding *Si*_edge atoms. Water hydrogen and oxygen atoms (not shown in this figure) are named *Hw* and *Ow* respectively in this study. (For interpretation of the references to colour in this figure legend, the reader is referred to the web version of this article.)

gallery for the uncharged (110) clay surface, and is consistent with the start of the bilayer of a water shown in previous classical simulations of clay minerals, such as Na-montmorillonite and Li-montmorillonite (Boek et al., 1995); see Fig. 2 for a visualization of the initial structure. Water molecules were then added until the density of water in the area unoccupied by the clay framework atoms was approximately 1.0 g/mL. For the (110) surface, 140 water molecules were added. For the (010) surface, 95 water molecules were added. To produce equilibrated input for *ab initio* molecular dynamics, preliminary classical molecular dynamics simulations were performed using the classical molecular dynamics code LAMMPS (Plimpton et al., 2015; Plimpton, 1995). The clay was described using the ClayFF forcefield (Cygan et al., 2004). For the terminal atoms added to saturate the dangling bonds, the charges were assigned to counterbalance the charge of the dangling bond (i.e. 0.525 for the terminal H in Si—O—H, where the

ClayFF oxygen atom partial charge is -1.05). The classical molecular dynamics simulations were performed in the NpT ensemble for approximately 5ns, at a temperature of 300K and with a pressure of 1atm. The z supercell dimension was kept fixed at 13.5 Å during these simulations; the x and y dimensions were allowed to vary. The clay atoms were fixed during these simulations. This provided the input to our CPMD simulations.

The final lattice parameters for the (110) face are: 18.34 Å × 20.68 Å × 13.5 Å; and for the (010) face: 10.34 Å × 27.84 Å × 13.5 Å. In total, the (110) and the (010) face systems contain 604 and 457 atoms respectively.

These systems are significantly larger than previously reported *ab initio* studies (which are comprised of 200–300 atoms (Churakov, 2007; Tazi et al., 2012)); as a consequence, the distance between the clay edges is increased and the interlayer spacing between the basal (001) surfaces of the clay is hydrated with a double layer of water. The

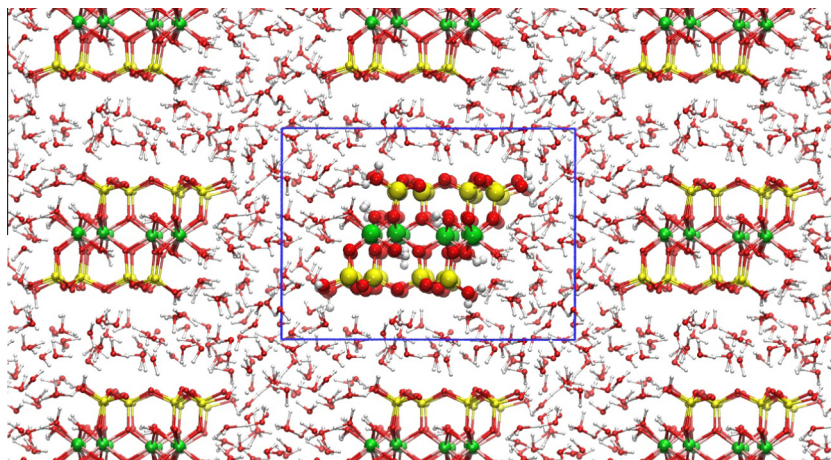


Fig. 2. The final snapshot from our *ab initio* MD simulation of the neutral (110) faces, after approximately 20ps of simulation, showing periodic replicas. O = red, H = white, Si = yellow and Al = green. The supercell periodic boundaries are indicated by the blue lines. The water molecules to the left and right of the (110) face are considered as micropore water; water molecules above the (001) surface are considered to be interlayer molecules. (For interpretation of the references to colour in this figure legend, the reader is referred to the web version of this article.)

larger size of the clay framework ensures that the charge sites due to isomorphous substitutions in the clay edge do not interact with their periodic images, and the large size of the micropore regions ensures that our findings do not suffer from the unintended consequences of confining the water molecules to very small pore volumes between clay edges.

The starting clay structures for the (110) and (010) face simulations are shown in Fig. 1a and b respectively. As there are 184 and 172 atoms in the clay structure for the (110) and (010) face systems respectively, we do not report the properties (bond distances, radial distribution functions etc.) for each individual atom in the clay framework. Instead, at the beginning of the simulation, we identify different atom types, depending on their chemical environment. The properties of the atoms for each type are averaged and used in further analysis. The atom types are indicated in Fig. 1a and b. A list of atom types and their description is given in the Supporting Information along with average clay framework bond distances from the *ab initio* MD simulations. The full simulation supercell, including all water molecules, is shown in Fig. 2 for the (110) surface and Fig. 12 for the (010) surface.

In this study, we consider both neutral and charged clay frameworks. We firstly performed *ab initio* molecular dynamics using the CPMD code on the neutral frameworks of the (110) and (010) surfaces. The (110) surface (and the equivalent -110 surface) has been determined by Churakov to have the lowest surface energy and is the largest component of the edge surfaces in a clay particle (Churakov, 2006). This estimation was based upon using DFT to calculate the energy of water sorption on different edge facets; when combined with the Wulff construction, this leads to the prediction that clay layer edges will be dominated by the (110) and (-110) faces. As isomorphous substitutions will comprise only a small fraction of edge

sites, we can assume that the (110) and (-110) faces will be the most stable with charged clays.

Our simulations of charged edges therefore concentrate on isomorphous substitutions in the (110) face. Two charged-layer systems were created: (1) a substitution of a single Si^{4+} ion by an Al^{3+} ion in the tetrahedral layer on the (110) surface, and (2) a substitution of a Al^{3+} ion by an Mg^{2+} ion in the tetrahedral layer. The charge compensating sodium counterion was placed in the middle of the opposite surface in the interlayer of the clay. These charged systems were created using a snapshot from the equilibrated (110) clay edge simulation.

This corresponds to the charged (110) silicate frameworks simulated by Liu et al. (2012) in their free energy calculations of proton dissociation from clay edges. Their study considered water molecules adjacent to the clay edge, but not in the clay interlayer. They found that for the (110) surface, substitution of Si by Al in the tetrahedral sheet of the clay edge (Si_{edge} in our nomenclature) leads to a very high pK_a and hence will remain protonated. Similarly, substitution of Al (Al_{oct.edge}) by Mg in the octahedral sheet leads to a $\text{Mg}(\text{OH})_2$ complex, again with a very high pK_a (Liu et al., 2014). Both types of isomorphous substitution were also observed to increase the pK_a on neighboring apical sites (o_{ap.edge}). In our study, with more extensive water coverage, we can observe the surface rearrangement that occurs (which due to the high pK_a should be on the timescale of our simulations) without the need to bias the simulation through a reaction coordinate required to calculate free-energies. For example, Churakov observed proton exchange on the hydrated (010) edge sites of neutral clays. Water molecules near the interface can rearrange to stabilize the products of the proton transfer reactions and lower the activation barrier required for the proton exchange (Churakov, 2007). In our case, with a more realistic structure of hydrated clays (a large micropore and interlayer

layer), we can examine proton exchange and water rearrangement as a function of isomorphic substitution.

We used several parameters to characterize the water structure. Firstly, we calculated the radial distribution function $g(r)$ between each of the clay atom types and the water atoms. Secondly, we calculated the atomic density profile perpendicular to the clay edges. This is computed as a function of the normal to the surface defined by the edge silicon atoms (the blue dotted lines in Fig. 1). Only water molecules with a z coordinate within that of the clay layer ± 1 Å are considered, to remove the interlayer molecules from the density profile. The hydrogen bonded network was computed at various snapshots during the *ab initio* simulations by defining a hydrogen bond as an O \cdots H distance less than 4 Å and O \cdots H–O angle greater than 140°.

For all the *ab initio* MD studies, the simulations were performed for between 12 and 20 ps with a fictitious electron mass equal to 800 a.u. and a timestep of 5 a.u. (0.12 fs). The simulations were performed in the *NVE* ensemble, with the temperature kept within 20 K of the desired temperature (300 K) through velocity rescaling in the equilibrium stages. All atoms were allowed to move during the *ab initio* MD simulations. Atomic positional data was collected every timestep and subsequently used for analysis. The generalized gradient approximation PBE (Lee et al., 1988; Becke, 1993; Perdew et al., 1996) was used for the exchange and correlation functionals. The energy cutoff for the plane-wave expansion of the wave function was 70 Rydberg. The large size of the cell meant Brillouin zone sampling was restricted to the Γ point. Medium-soft normconserving pseudopotentials were used, based on the Troullier–Martins (TM) scheme (Troullier and Martins, 1991).

3. AB INITIO MOLECULAR DYNAMICS RESULTS

Using *ab initio* simulation we can study the hydration of both the clay interlayer and the edges, allowing us to determine the difference in water structure between the micropore and interlayer regions. We firstly consider the water structure in the vicinity of the neutral clay edge and subsequently the changes in interfacial structure associated with isomorphic substitution. We are also able to identify acidic sites through dissociation mechanisms and observe reorganization of the surface.

3.1. Neutral (110) face

A snapshot from our *ab initio* MD simulation of the neutral (110) face is shown in Fig. 2. Periodic images are also displayed to illustrate the hydrated nature of each clay layer. No proton dissociation was seen during the lifetime of our simulation of the neutral (110) face, consistent with the simulations of Liu et al. (2012). As observed in visualizations, we find that the hydroxyl groups on the (110) edge surface are flexible, allowing motions that result in hydrogen bonding to water molecules in either the micropore or interlayer region. This is confirmed by the radial distribution function and coordination number of the edge hydroxyl atoms (ob_edge and ho_edge in our nomenclature) with water (Fig. 3); the ho_edge coordination with water hydrogen atom is 1 at a distance of 2.5 Å, indicating stable hydrogen bond formation (in the previous study of Liu et al., due to the absence of interlayer water, the coordination number was significantly lower at approximately 0.5 (Liu et al., 2012), while in the study of Churakov the coordination number was either 0.98 or 0.01 depending on whether the ho_edge atom pointed into the micropore or not (Churakov, 2007)). This is the defining feature of the (110) face from our *ab initio* MD simulations: the flexibility of the edge hydroxyl atoms creates a variety of hydrogen bonded networks both in the interlayer and micropore regions.

To further investigate, we have taken a representative snapshot from the (110) face simulation and analyzed the hydrogen bonded networks that stretch across the opening of the clay galleries. In Fig. 4 we show some of these networks, spanning two or three water molecules. We see that when the ho_edge atom is pointing towards the interlayer, it forms a hydrogen bonded network that terminates, via two water molecules, on either the basal oxygen atoms or the ob_edge atoms on the opposite surface (Fig. 4a). When the ho_edge atom is pointing towards the micropore spacing, a network exists that can terminate on the opposite surface, via three water molecules (Fig. 4b). This highly orientated network across the interface region may provide a barrier to water diffusion from the micropore into the interlayer, although this can not be confirmed from the relatively short timescales possible with AIMD. Within periodic clay models (i.e. without clay edges), the interlayer

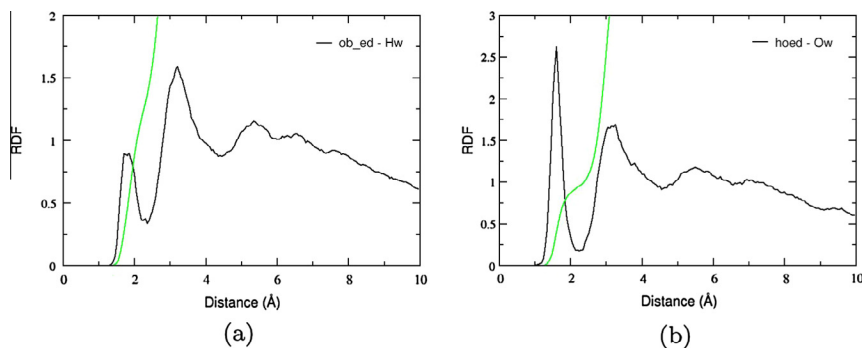


Fig. 3. Radial distribution functions and integrals for hydroxyl groups on the neutral (110) face with water atoms: (a) ob_edge and water hydrogen atoms, (b) ho_edge and oxygen water atoms.

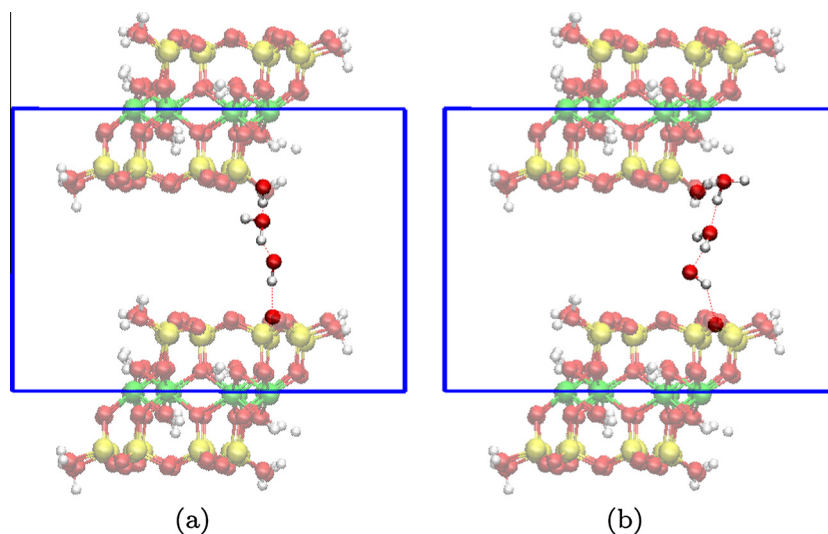


Fig. 4. An illustration of the hydrogen bonded networks found in a representative snapshot from the *ab initio* MD simulation of the (110) face. The hydrogen bonds are indicated by red dashed lines and the periodic boundaries of the simulation supercell are solid blue line. (a) A hydrogen bonded network between `ho_edge` atoms and basal oxygen atoms (`ob`) on the opposite clay surface, consisting of two water molecules; (b) a hydrogen bonded network between `ho_edge` atoms and basal oxygen atoms (`ob`) on the opposite clay surface, consisting of three water molecules. (For interpretation of the references to color in this figure legend, the reader is referred to the web version of this article.)

water molecules have been shown to predominantly form hydrogen bonds to themselves rather than the clay surface (unless in the vicinity of a charge site or aqueous ion) (Boek and Sprik, 2003). Such an arrangement is not necessarily compatible with the edge hydroxyl hydrogen-bonded network due to their differing alignment.

To demonstrate this, Fig. 5 shows a “heat map” of the water hydrogen atoms in the xz plane. We see a significant density above each of the edge hydroxyl groups and on the basal oxygen atoms on the opposite surface (highlighted by arrows), illustrating the hydrogen bonding network stretching across the interlayer. There is little hydrogen atom density above the remaining basal oxygen atoms on the surface, indicating that the majority of hydrogen bonds to the surface are due to networks originating in the edge hydroxyl atoms.

The *ab initio* MD simulations can also be used to elucidate the structure of water molecules adsorbed on the (110) face. Using the atomic density profiles perpendicular to the (110) surface, we can identify several distinct adsorption patterns, corresponding to the edge atoms acting as either hydrogen bond acceptors or donors. These adsorption sites produce distinct peaks in the density profile, shown in Fig. 6, at 1.85 Å, 2.65 Å and 3.4 Å from the (110) surface. The first peak, at 1.85 Å, is due to water molecules forming a bond with the exposed 5 coordinate aluminum atom (`Al_oct_edge`) on the (110) surface. This can be interpreted as being caused by the 5 coordinate aluminum ion acting as a Lewis acid. The second peak, at 2.65 Å, is due to both the exposed apical oxygen atom (`o_ap_edge`) acting as a hydrogen bond donor and the clay framework hydroxyl atoms acting as a hydrogen bond acceptor. The final peak, at 3.4 Å, is due to water molecules forming hydrogen bonds with the silicate hydroxyl atoms (`ho_edge`). Similar

arrangements of adsorbed water molecules were seen for Liu et al. (2012) and Churakov (2007), although due to the greater amount of water (including interlayer water

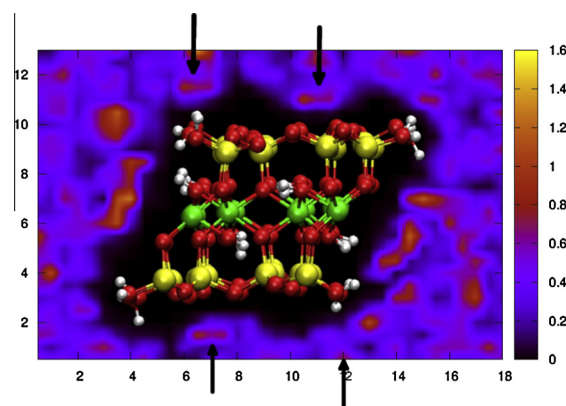


Fig. 5. Heat map showing the density of water hydrogen atoms in the xz plane, averaged over $0.5 \text{ \AA} \times L_y \times 0.5 \text{ \AA}$ volumes and interpolated to produce a smooth image. The x and y units are in Angstroms. The color key refers to the average number of water hydrogen atoms found within the $0.5 \text{ \AA} \times L_y \times 0.5 \text{ \AA}$ volume. A representative snapshot of the (110) face is also shown. Indicated by the arrows are regions where hydrogen bonding with the clay surface is high, corresponding to the hydrogen bonded networks described in Fig. 4. The water molecules bound to the 5-coordinate Al atom (`Al_oct_edge`) remain in this position through the simulation and therefore show the highest density. Water molecules further away from the surface show greater movement, and hence their densities are more spread out. (For interpretation of the references to color in this figure legend, the reader is referred to the web version of this article.)

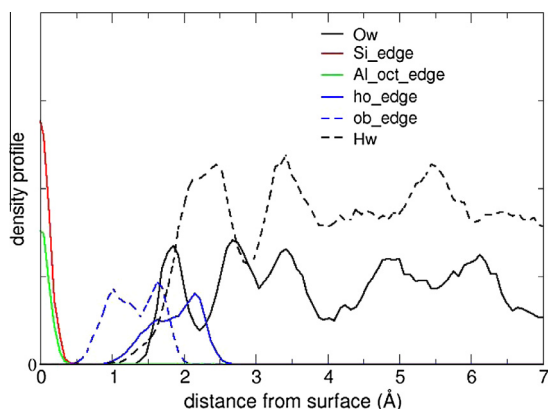


Fig. 6. The density profile of atom types from the (110) surface, defined as the perpendicular distance from the blue dotted lines in Fig. 1. (For interpretation of the references to color in this figure legend, the reader is referred to the web version of this article.)

molecules) in our study, we find the edge hydroxyl atoms form a much greater number of hydrogen bonds. As illustrated in the schematic diagram in Fig. 7, these adsorbed water molecules can form hydrogen bonds amongst themselves as well. In summary, the numerous interaction sites of the (110) face, combined with a favorable geometry for hydrogen bonding to other water molecules, lead to a strongly bound layer of adsorbed water on the surface. Due to the flexible hydroxyl groups, it is possible for this network to extend upwards or downwards to an adjacent clay layer within a tactoid.

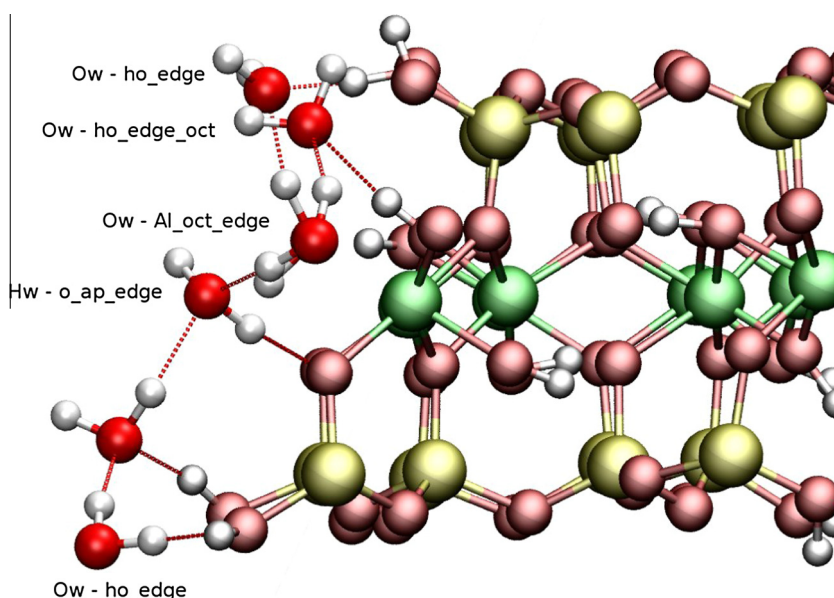


Fig. 7. Schematic diagram illustrating typical conformations of water molecules adsorbed on the (110) face. The surface atom type and the hydrogen or oxygen water atom involved in the interaction are shown in the figure. These conformations lead to the distinct peaks in the density profile perpendicular to the clay surface for H_w and O_w atoms (Fig. 6). Hydrogen bonds are shown as dashed red lines. (For interpretation of the references to colour in this figure legend, the reader is referred to the web version of this article.)

3.2. Isomorphous substitution in the clay (110) surface tetrahedral layer

The final snapshot from our *ab initio* molecular dynamics simulation of the (110) surface with a silicon atom substituted by an aluminum atom in the tetrahedral layer of the clay is shown in Fig. 8. Several things should be noted: the sodium ion was initially placed in the interlayer, in the middle of the opposite surface. By the end of our simulation (approximately 18 ps), the sodium ion had moved to the edge of the clay layer. We find that the hydration shell of the sodium ion is composed of two oxygen atoms from the clay framework (one basal oxygen atom (O_b) and one $\equiv\text{Si}-\text{OH}$ edge oxygen atom), with the remainder of the shell made up of water molecules. It should be noted that the final location of the sodium atom is where there is little hydrogen atom density in the uncharged system, as shown in Fig. 5. This indicates a preference for the sodium ion not to perturb the hydrogen bonding network.

In our simulations, we observe that the apical oxygen atom ($o_{\text{ap_edge}}$), bound to the site of isomorphous substitution in the tetrahedral layer, immediately extracts a proton from the nearby water molecule. This is consistent with the study of Liu et al., who calculated that, for a clay with no water in the interlayer, the $\text{p}K_a$ of the apical oxygen atom of a clay is 10.2, indicating it is protonated under normal pH (Liu et al., 2014). As in Ref. Liu et al. (2012), we also observe that in turn this water molecule extracts a proton from a water molecule bound to the octahedral aluminum atom ($\text{Ow}-\text{Al}_{\text{oct_edge}}$). This is illustrated in Fig. 9. The result is that the octahedral aluminum ($\text{Al}_{\text{oct_edge}}$) is now bound by two OH groups, rather than one OH group

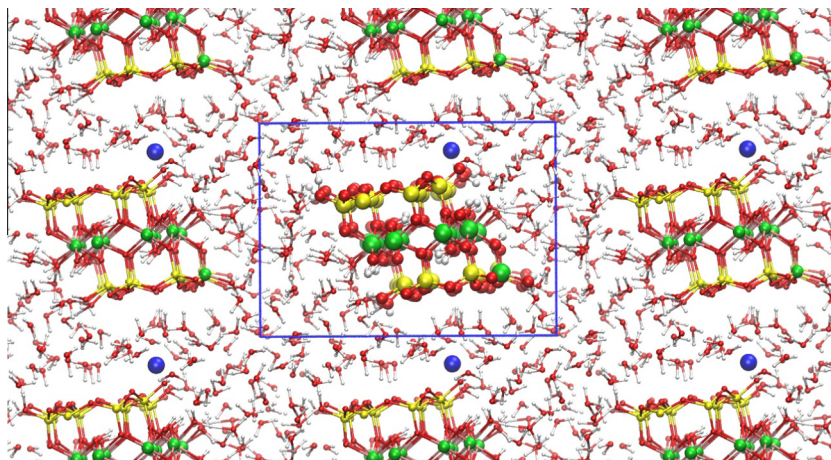


Fig. 8. A snapshot from the *ab initio* MD simulation of the (110) face with an aluminium atom substitution in the tetrahedral layer, viewed in the *xz* plane and showing the nearest periodic replicas. The atom colors are as in Fig. 1, with the sodium ion in blue. Periodic boundaries are solid blue lines. (For interpretation of the references to colour in this figure legend, the reader is referred to the web version of this article.)

and one water molecule in the uncharged case. This surface reorganization, via the hydrogen bonded network, illustrates the Lewis acidity associated with the 5 coordinate aluminum atom and the Brønsted basicity of the adjacent exposed apical oxygen. Here, these two functions work cooperatively to promote the proton rearrangement on the (110) face. The catalytic activity of clays has been suggested to be related to the aluminum ions on the crystal edges (Stackhouse et al., 2001); here we see that sites of isomorphous substitution increase this reactivity such that it is visible on the timescale of our *ab initio* MD simulations (<20 ps).

This proton movement also changes the nature of the adsorbed water on the (110) surface in the vicinity of the charge site; the exposed apical oxygen atom now acts as a hydrogen bond donor rather than acceptor. As a result of this, water molecules adsorb to the basal surface oxygen

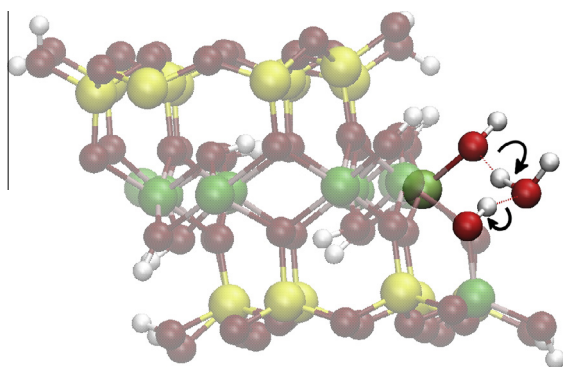


Fig. 9. The mechanism of proton hopping on the (110) face with an isomorphous substitution in the tetrahedral layer (the aluminum atom (green)). The water molecule bound to the nearest aluminum is deprotonated, and hops, via a single water molecule, to the exposed apical oxygen atom on the surface. This illustrates the Lewis acidity associated with the 5 coordinate aluminum atom and the Brønsted basicity of the adjacent exposed apical oxygen. (For interpretation of the references to colour in this figure legend, the reader is referred to the web version of this article.)

atoms on both the upper and lower tetrahedral layers near the edge hydroxyl groups (a snapshot illustrating this is shown in Supporting Information). This hydrogen bonded network is only possible due to water molecules in the interlayer spacing, and we can infer that full hydration leads to greater stability of the tetrahedral substituted (110) face after proton rearrangement. Beyond the vicinity of the charge site, the density profile of adsorbed water is identical to that of the neutral (110) face.

3.3. Isomorphous substitution in the clay (110) surface octahedral layer

The final snapshot from our *ab initio* molecular dynamics simulation of the (110) surface, with an aluminum ion substituted for a magnesium ion in the octahedral layer of the clay, is shown in Fig. 10. Analogous to the tetrahedrally charged (110) surface, during the simulation the sodium ion moves from the centre of the interlayer to reside on the edge of the basal surface, bound by edge hydroxyl oxygen atoms and water molecules.

We observe no bond breaking or formation in this system; however, the radial distribution function of the exposed apical oxygen atom (*o_ap_edge*) bound to the magnesium ion (see Supporting Information) shows that this ion forms hydrogen bonds with two water molecules compared to approximately one hydrogen bond by the other exposed apical oxygen atoms on the (110) face. In Fig. 11, a snapshot from the *ab initio* simulation illustrates the exposed apical oxygen atom forming hydrogen bonds with two water molecules. We also observe that the ≡Si–OH edge groups nearest this apical oxygen point towards the interlayer, forming hydrogen bonds with interlayer water molecules. Compared with the foregoing observations, the lack of any deprotonation mechanism on the timescale of our simulation suggests that the reactivity of the clay edges containing isomorphous substitution in the octahedral layer is less than isomorphous substitution in the tetrahedral layer. This is again consistent with the study of Liu et al., who calculated a pK_a of 4.2 (Liu et al., 2014).

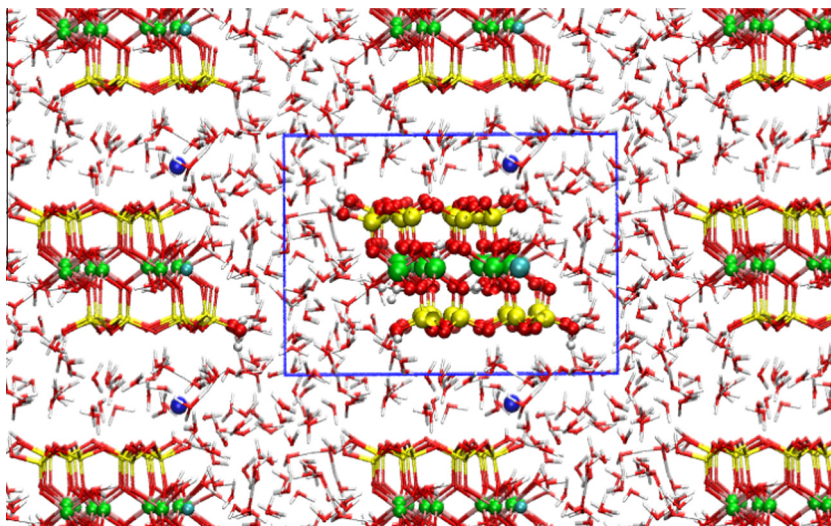


Fig. 10. A snapshot from the *ab initio* MD simulation of (110) face with a magnesium ion substitution in the octahedral layer (aqua color), viewed in the *xz* plane and showing the nearest periodic replicas. The atom colors are as in Fig. 1, with the sodium ion in blue. Periodic boundaries are solid blue lines. (For interpretation of the references to colour in this figure legend, the reader is referred to the web version of this article.)

3.4. Neutral (010) face

In the previous sections, we have seen that the (110) face contains stable surface hydroxyl groups that form a variety of hydrogen bonded networks which span clay layers and their periodic images. The situation with the (010) face is very different. A snapshot from the *ab initio* MD simulation of the (010) face system is shown in Fig. 12. On the time-scale of our simulations (approximately 20 ps), the edge tetrahedral hydroxyl groups are not stable; we observe the deprotonation of two of these groups. We conclude that the (010) face tetrahedral hydroxyl group is a much stronger Brønsted acid than the (110) face hydroxyl group. This deprotonation is followed by the protonation of an adjacent octahedral hydroxyl group, forming a second water

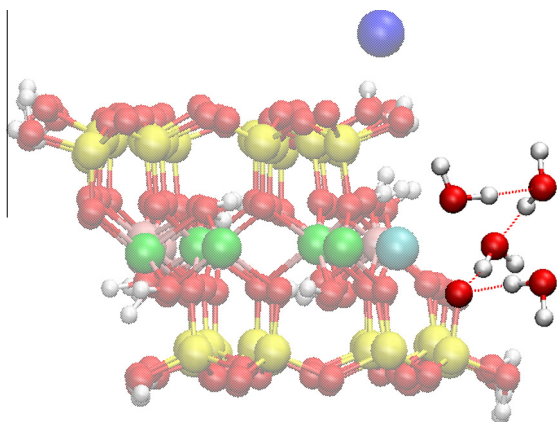


Fig. 11. The arrangement of water molecules near the site of the isomorphic substitution in the octahedral layer of the (110) face. We see that there are two water molecules forming hydrogen bonds with the O_{ap_edge} .

molecule bound to the 5 coordinate aluminum ion on the surface. This proton rearrangement occurs via two water molecules in the micropore region, and is illustrated in Fig. 13.

The deprotonated hydroxyl group anion is stabilized by the interaction of four water molecules: two from the inter-layer region and two from the micropore region. A snapshot showing this arrangement can be found in the Supporting Information. Similar deprotonation states were observed by Churakov (2007), although he saw the eventual re-protonation of the deprotonated hydroxyl group; here, we do not observe such an event, probably due to the additional stabilisation of the anion by the interlayer water molecules. Similar deprotonation and eventual re-protonation events were seen for Mg substituted (010) faces by Liu et al. (2012), but not for the uncharged 010 face. As a further illustration of the reactivity of the (010) face surface hydroxyls, we also observed a reversible deprotonation of a surface hydroxyl group (of approximately 1 ps duration). From visualization of the simulation we observed that a proton could not hop to the octahedral hydroxyl as before, due to the arrangement of the water molecules in the vicinity of that region in the simulation. Instead, these protons returned to their original hydroxyl oxygen atoms.

The structure of the water molecules adsorbed on the (010) face is also very different to the (110) face. Overall, the number of hydrogen bonds formed by the $\equiv Si-OH_{ob_edge}$ group is reduced compared to the (110) face, to approximately 0.6 at the first minimum in the radial distribution function (2.25 Å), compared to approximately 1.0 for the (110) face. There is, however, a significant amount of hydrogen bonding from the octahedral edge hydroxyls, amounting to 0.3 at 2.25 Å, which is not present in the (110) face as they are much further away in the clay framework. In Fig. 14 we show the density profile perpendicular

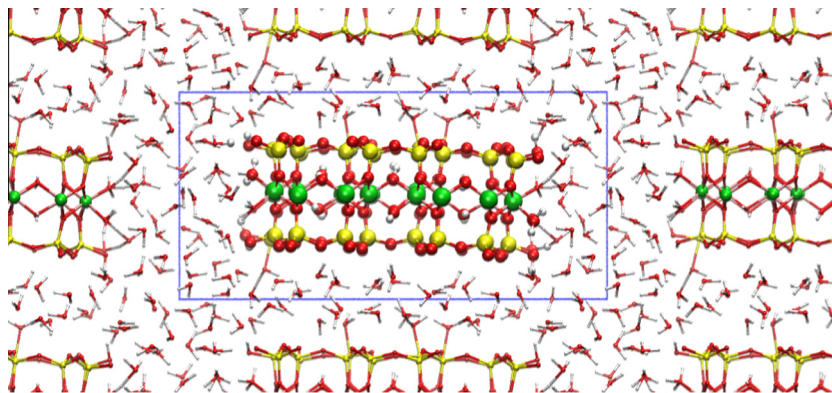


Fig. 12. The final snapshot from our *ab initio* MD simulation of the neutral (010) faces in the yz plane, showing periodic replicas. O = red, H = white, Si = yellow and Al = green. The supercell periodic boundaries are indicated by the blue lines. (For interpretation of the references to colour in this figure legend, the reader is referred to the web version of this article.)

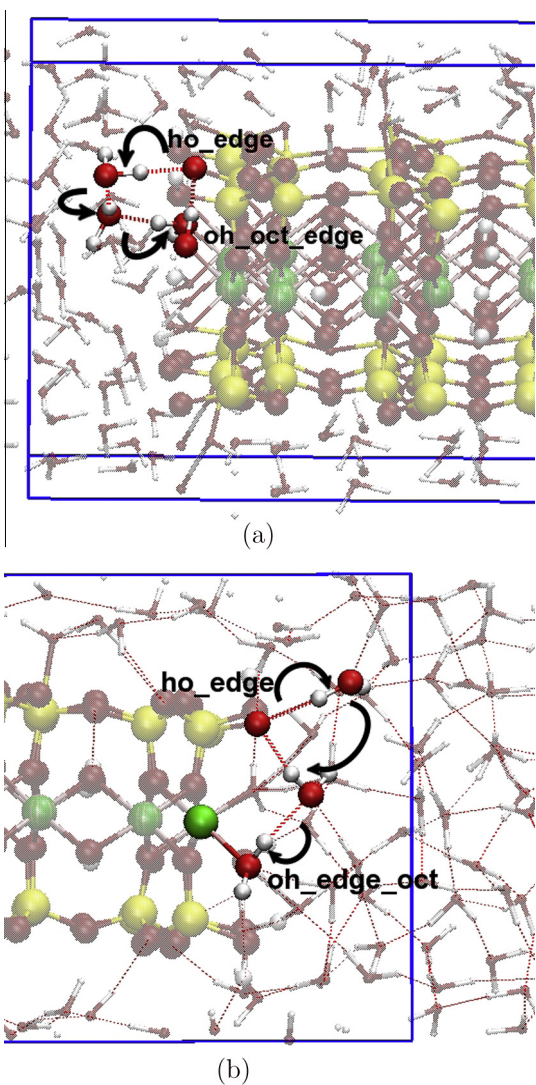


Fig. 13. Proton hopping on the (010) surface: *ho_edge* is deprotonated and *oh_oct_edge* is protonated. This mechanism proceeds via two water molecules. (a) *oh_oct_edge* is directly below the *ho_edge* and (b) *oh_oct_edge* is further below the *ho_edge* group.

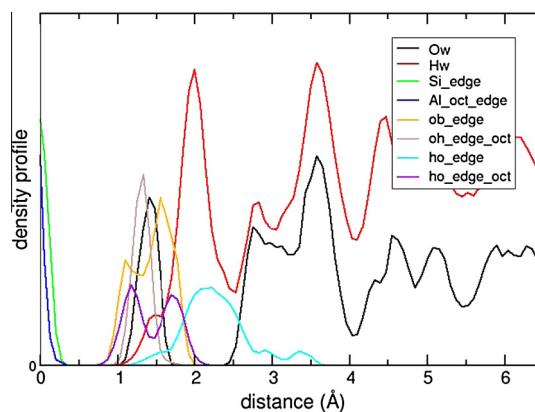


Fig. 14. The atomic density profile perpendicular to the (010) face, defined as the distance perpendicular from the blue dotted line in Fig. 1b. The atom types are indicated in Fig. 1b. Hydrogen bonds are indicated by red dotted lines. (For interpretation of the references to colour in this figure legend, the reader is referred to the web version of this article.)

to the (010) surface; we observe only a single peak of *ho_edge* atoms (albeit with a tail at large distances due to the deprotonation). We see a large peak in the *O_w* peak at 1.45 Å which corresponds to water molecules forming bonds with the five coordinate aluminum ions.

Unlike the (110) surfaces, we find there is no hydrogen bonded network which spans the interlayer spacing through either two or three bridging water molecules. This indicates that the hydrogen bonded network extends out from the (110) surface, into the micropore, rather than directly across the interlayer spacing.

4. CONCLUSIONS

We have used molecular dynamics at the quantum level to understand the role of clay edges in the micropore/interlayer interface. Our models have included both interlayer water and a large micropore region, providing a realistic description of a hydrated clay. It is clear that the properties

of clay edges and the associated interfacial structures are complex; we observe the edges behaving as both Brønsted acids and bases, as well as Lewis acids, thus revealing the amphoteric nature of the clay edge. Although our simulations are large by *ab initio* MD standards, they are, of course, of limited size and timescale. We can not observe processes with length and timescales greater than approximately 20 Å and 20 ps respectively. With unlimited computational resources, we would use statistical mechanical approaches (such as ensemble or free energy methods) to sample longer time and length scales. However, *ab initio* MD can still give considerable insight into the reactivity of the clay edges; from the observations in our simulations we can propose plausible pH dependent structures and catalytic sites. As our simulations show, the complex behavior of clay edges is one of the reasons for the difficulty in assigning the reactive groups from titration experiments due to many microscopic sites contributing to the overall behavior.

In our *ab initio* MD, the (110) face is particularly stable on the timescale of our simulations, with a well defined structure of adsorbed water molecules and an extensive hydrogen bonding network involving the edge hydroxyl atoms and spanning across the interlayer. The reactivity of the (110) edge is increased with isomorphic substitutions on the edge, especially those in the tetrahedral layer, which lead to the edge acting as a Brønsted base, extracting a proton from a neighboring water molecule. The high proton affinity of this oxygen atom (as evidenced by proton abstraction occurring during our simulations) indicates that this atom can act as a relatively strong base. This isomorphic substitution also causes a water molecule bound to the exposed aluminum ion to behave as a Brønsted acid, with the donated proton hopping to the site of Brønsted basicity.

We can therefore postulate that the isomorphic substitutions will affect the amount of proton uptake within clay edge structures: the higher the degree of tetrahedral substitutions, the greater the number of Brønsted base sites. Our simulations suggest these will be protonated even at neutral pH.

With isomorphic substitutions in the octahedral layer of the (110) edge, the exposed apical oxygen becomes a hydrogen bond donor to two water molecules (as opposed to one for the neutral surface). This suggests that at low pH (i.e. acid activated clay) this exposed oxygen would be protonated. This is especially important as the catalytic ability of montmorillonite clay is known to increase after acid treatment (Briones-Jurado and Agacino-Valdés, 2009). In its protonated state, this could also be the site of a Brønsted acid; as we did not see this oxygen atom become protonated during our simulation we infer that the proton affinity is less than that of the oxygen atom adjacent to a tetrahedral layer isomorphic substitution and could be a candidate for proton donation in a catalytic acid treated clay.

Previous studies have indicated that the edges of clay platelets should be dominated by (110) surfaces; however, the *ab initio* simulation of the (010) edge indicates that this surface, although less prevalent, is much more reactive, with the edge SiOH hydroxyl groups acting as Brønsted

acids. When the clay is fully hydrated, the deprotonated anion is stabilized by interactions with water molecules in both the interlayer and micropore regions. Previous studies of the (010) surfaces of clay with no interlayer water have estimated the SiOH site to have a pK_a of 6.8 ± 0.4 (Tazi et al., 2012). Although our findings are purely observational, the number of SiOH groups which deprotonate in our simulations (half of the total) indicates that when fully hydrated, the pK_a may be significantly lower due to the additional stabilization of the deprotonated anion by the interlayer and micropore water molecules. We can hypothesize that any acid catalyzed reaction involving the (010) surface will be a function of water content (via clay swelling).

An explanation for the lack of deprotonation events on the neutral (110) surface is that the extensive hydrogen bonding network of the adsorbed water molecules allows the hydroxyl groups on the surface to form the maximum number of hydrogen bonds. An expansive hydrogen bonding network of this kind leads to stability of possible dissociation sites in their protonated states; such a hydrogen bonded network is missing from the (010) surface. The flexibility of the edge hydroxyl atoms and the hydrogen bonded networks across the pore and interlayer spacings from the (110) edge infer that such behavior would be seen regardless of the separation of the clay layers. This will be the focus of future research.

The detailed description of the hydrogen bonded network and the associated interfacial structures we have encountered will provide insights and information with which to develop force-field parameters for classical molecular dynamics simulations. Such forcefields must capture the interfacial behavior and also the relaxation of the clay framework at edge sites. We are currently developing these parameters, which can then be further propagated to higher levels of simulation, such as coarse-grained molecular dynamics (Suter et al., 2015). Furthermore, specialized classical molecular dynamics forcefields such as ReaxFF can handle both bond breaking and formation; these have been previously used for clay edges (Pitman and Van Duin, 2012) but can in future be optimized to recreate the proton reorganisation on the various faces or the behavior at various pH. Classical and coarse-grained MD will allow us to simulate much longer timescales, such that we can study the role of clay edges and pore shape in affecting the diffusional behavior of water between the micropore and interlayer, as well as the desorption/adsorption properties of the clay edges (Cygan et al., 2009; Rotenberg et al., 2007).

ACKNOWLEDGEMENTS

This research was supported through a grant from the Qatar National Research Fund (QNRF) of Qatar Foundation, National Priorities Research Program (grant number 09-26-01-048). Our work made use of the facilities of HECToR, the UK's national high-performance computing service, which is provided by UoE HPCx Ltd at the University of Edinburgh, Cray Inc and NAG Ltd, and funded by the Office of Science and Technology through EPSRC's High End Computing Programme. Access to HECToR was through grants EP/F00521/1, EP/E045111/1, EP/I017763/1 and the UK Consortium on

Mesoscopic Engineering Sciences (EP/L00030X/1). We also made use of High Performance Computing facilities at University College London.

APPENDIX A. SUPPLEMENTARY DATA

Additional radial distribution functions of clay edge atoms and a full description of clay edge atom types. Supplementary data associated with this article can be found, in the online version, at <http://dx.doi.org/10.1016/j.gca.2015.07.013>. These data include MOL files and InChiKeys of the most important compounds described in this article.

REFERENCES

- Accelrys Software Inc (2007) Discovery studio modeling environment, release 3.0.
- Anderson R. L., Ratcliffe I., Greenwell H. C., Williams P. A., Cliffe S. and Coveney P. V. (2010) Clay swelling – a challenge in the oilfield. *Earth. Sci. Rev.* **98**(3–4), 201–216.
- Becke A. D. (1993) Density-functional thermochemistry. III. The role of exact exchange. *J. Chem. Phys.* **98**(7), 5648–5652.
- Bergaya F. and Lagaly G. (2013) *Handbook of Clay Science*. vol. 5. Newnes.
- Bickmore B. R., Rosso K. M., Nagy K. L., Cygan R. T. and Tadanier C. J. (2003) Ab initio determination of edge surface structures for dioctahedral 2:1 phyllosilicates: implications for acid-base reactivity. *Clay. Clay Min.* **51**(4), 359–371.
- Boek E. S. and Sprik M. (2003) Ab initio molecular dynamics study of the hydration of a sodium smectite clay. *J. Phys. Chem. B* **107**(14), 3251–3256.
- Boek E. S., Coveney P. V. and Skipper N. T. (1995) Monte Carlo molecular modeling studies of hydrated Li-, Na-, and K-smectites: understanding the role of potassium as a clay swelling inhibitor. *J. Am. Chem. Soc.* **117**, 12608.
- Boek E. S., Coveney P. V. and Skipper N. T. (1995) Molecular modeling of clay hydration: a study of hysteresis loops in the swelling curves of sodium montmorillonites. *Langmuir* **11**, 4629.
- Boulet P., Greenwell H. C., Stackhouse S. and Coveney P. V. (2006) Recent advances in understanding the structure and reactivity of clays using electronic structure calculations. *J. Mol. Struct. Theochem.* **762**(1), 33–48.
- Bridgeman C. H. and Skipper N. T. (1997) A Monte Carlo study of water at an uncharged clay surface. *J. Phys. Cond. Matt.* **9**(20), 4081.
- Brindley G. W. and Brown G. (1980) *Crystal Structures of Clay Minerals and their X-ray Identification*. Mineralogical Society, London.
- Briones-Jurado C. and Agacino-Valdés E. (2009) Brønsted sites on acid-treated montmorillonite: a theoretical study with probe molecules. *J. Phys. Chem. A* **113**(31), 8994–9001.
- Chang F. R. C., Skipper N. T. and Sposito G. (1995) Computer simulation of interlayer molecular structure in sodium montmorillonite hydrates. *Langmuir* **11**, 2734.
- Chang F. R. C., Skipper N. T. and Sposito G. (1997) Monte carlo and molecular dynamics simulations of interfacial structure in lithium-montmorillonite hydrates. *Langmuir* **13**, 2074.
- Chang F. R. C., Skipper N. T. and Sposito G. (1998) Monte Carlo and molecular dynamics simulations of electrical double-layer structure in potassium-montmorillonite hydrates. *Langmuir* **14**, 1201.
- Chen B., Evans J. R., Greenwell H. C., Boulet P., Coveney P. V., Bowden A. A. and Whiting A. (2008) A critical appraisal of polymer–clay nanocomposites. *Chem. Soc. Rev.* **37**(3), 568–594.
- Churakov S. V. (2006) Ab initio study of sorption on pyrophyllite: structure and acidity of the edge sites. *J. Phys. Chem. B* **110**(9), 4135–4146.
- Churakov S. V. (2007) Structure and dynamics of the water films confined between edges of pyrophyllite: a first principle study. *Geochim. Cosmochim. Acta.* **71**(5), 1130–1144.
- Cygan R. T., Liang J.-J. and Kalinichev A. G. (2004) Molecular models of hydroxide, oxyhydroxide, and clay phases and the development of a general force field. *J. Phys. Chem. B* **108**(4), 1255–1266.
- Cygan R. T., Greathouse J. A., Heinz H. and Kalinichev A. G. (2009) Molecular models and simulations of layered materials. *J. Mater. Chem.* **19**(17), 2470–2481.
- Delville A. (1991) Modeling the clay-water interface. *Langmuir* **7**(3), 547–555.
- Giese R. F. and Van Oss C. J. (2002) *Colloid and Surface Properties of Clays and Related Minerals*. CRC Press.
- Greenwell H. C., Jones W., Coveney P. V. and Stackhouse S. (2006) On the application of computer simulation techniques to anionic and cationic clays: a materials chemistry perspective. *J. Mater. Chem.* **16**(8), 708–723.
- Hutter J., Alavi A., Deutsch T., Bernasconi M., Goedecker S., Marx D., Tuckerman M., Parrinello M. (2011) Car-Parrinello molecular dynamics, version 3.15.1, MPI Solid State Research Institute in Stuttgart and the IBM Research Laboratory Zurich.
- Karaborni S., Smit B., Heidug W., Urai J. and Van Oort E. (1996) The swelling of clays: molecular simulations of the hydration of montmorillonite. *Science* **271**, 1102.
- Lee C., Yang W. and Parr R. (1988) Development of the Colle–Salvetti correlation-energy formula into a functional of the electron density. *Phys. Rev. B* **37**, 785–789.
- Liu X., Lu X., Meijer E. J., Wang R. and Zhou H. (2012) Atomic-scale structures of interfaces between phyllosilicate edges and water. *Geochim. Cosmochim. Acta.* **81**, 56–68.
- Liu X., Cheng J., Sprik M., Lu X. and Wang R. (2014) Surface acidity of 2:1-type dioctahedral clay minerals from first principles molecular dynamics simulations. *Geochim. Cosmochim. Acta.* **140**, 410–417.
- Marry V. and Turq P. (2003) Microscopic simulations of interlayer structure and dynamics in bihydrated heteroionic montmorillonites. *J. Phys. Chem. B* **107**(8), 1832–1839.
- Marry V., Rotenberg B. and Turq P. (2008) Structure and dynamics of water at a clay surface from molecular dynamics simulation. *Phys. Chem. Chem. Phys.* **10**(32), 4802–4813.
- Morrow C. P., Yazaydin A. Ö., Krishnan M., Bowers G. M., Kalinichev A. G. and Kirkpatrick R. J. (2013) Structure, energetics, and dynamics of smectite clay interlayer hydration: molecular dynamics and metadynamics investigation of Na-hectorite. *J. Phys. Chem. C* **117**(10), 5172–5187.
- Murray H. H. (2000) Traditional and new applications for kaolin, smectite, and palygorskite: a general overview. *Appl. Clay Sci.* **17**(5), 207–221.
- Newman A. C. D. (1987) *Chemistry of Clays and Clay Minerals*. Mineralogical Society.
- Perdew J. P., Burke K. and Ernzerhof M. (1996) Generalized gradient approximation made simple. *Phys. Rev. Lett.* **77**(18), 3865.
- Pitman M. C. and Van Duin A. C. (2012) Dynamics of confined reactive water in smectite clay–zeolite composites. *J. Am. Chem. Soc.* **134**(6), 3042–3053.
- Plimpton S. (1995) Fast parallel algorithms for short-range molecular dynamics. *J. Comp. Phys.* **117**(1), 1–19.
- Plimpton S., Crozier P., Thompson A. (2015) LAMMPS-large-scale atomic/molecular massively parallel simulator, Sandia National Laboratories.

- Rotenberg B., Marry V., Vuilleumier R., Malikova N., Simon C. and Turq P. (2007) Water and ions in clays: unraveling the interlayer/micropore exchange using molecular dynamics. *Geochim. Cosmochim. Acta* **71**(21), 5089–5101.
- Rotenberg B., Marry V., Malikova N. and Turq P. (2010) Molecular simulation of aqueous solutions at clay surfaces. *J. Phys. Condens. Matter*. **22**(28), 284114.
- Sposito G., Skipper N. T., Sutton R., Park S.-H., Soper A. K. and Greathouse J. A. (1999) Surface geochemistry of the clay minerals. *Proc. Natl. Acad. Sci.* **96**(7), 3358–3364.
- Stackhouse S., Coveney P. V. and Sandre E. (2001) Plane-wave density functional theoretic study of formation of clay-polymer nanocomposite materials by self-catalyzed in situ intercalative polymerization. *J. Am. Chem. Soc.* **123**, 11764.
- Suter J. L., Boek E. S. and Sprik M. (2008) Adsorption of a sodium ion on a smectite clay from constrained ab initio molecular dynamics simulations. *J. Phys. Chem. C* **112**(48), 18832–18839.
- Suter J. L., Coveney P. V., Anderson R. L., Greenwell H. C. and Cliffe S. (2011) Rule based design of clay-swelling inhibitors. *Ener. Env. Sci.* **4**(11), 4572–4586.
- Suter J. L., Sprik M. and Boek E. S. (2012) Free energies of absorption of alkali ions onto beidellite and montmorillonite surfaces from constrained molecular dynamics simulations. *Geochim. Cosmochim. Acta* **91**, 109–119.
- Suter J. L., Groen D. and Coveney P. V. (2015) Chemically specific multiscale modeling of clay - polymer nanocomposites reveals intercalation dynamics, tactoid self-assembly and emergent materials properties. *Adv. Mater.* **27**(6), 966–984.
- Tazi S., Rotenberg B., Salanne M., Sprik M. and Sulpizi M. (2012) Absolute acidity of clay edge sites from ab-initio simulations. *Geochim. Cosmochim. Acta* **94**, 1–11.
- Tournassat C., Neaman A., Villieras F., Bosbach D. and Charlet L. (2003) Nanomorphology of montmorillonite particles: estimation of the clay edge sorption site density by low-pressure gas adsorption and AFM observations. *Amer. Miner.* **88**(11–12), 1989–1995.
- Troullier N. and Martins J. (1991) Efficient pseudopotentials for plane-wave calculations. *Phys. Rev. B* **43**, 1993.

Associate editor: Jean Francois Boily